THE JOURNAL OF PHYSICAL CHEMISTRY C

pubs.acs.org/JPCC Article

Surface Segregation Across Ternary Alloy Composition Space: $Cu_xAu_yPd_{1-x-y}$

Chunrong Yin, Zhitao Guo, and Andrew J. Gellman*

Cite This: J. Phys. Chem. C 2020, 124, 10605−10614 Read Online

ACCESS | Metrics & More | Article Recommendations | Supporting Information

ABSTRACT: Surface segregation is a phenomenon common to all multicomponent materials and one that plays a critical role in determining their surface properties. Comprehensive studies of surface segregation versus bulk composition in ternary alloys have been prohibitive because of the need to study many different compositions. In this work, high-throughput low-energy He^+ ion-scattering spectra and energy-dispersive X-ray spectra were collected from a $Cu_xAu_yPd_{1-x-y}$ composition spread alloy film under ultrahigh vacuum conditions. These have been used to quantify surface segregation across the entire $Cu_xAu_yPd_{1-x-y}$ composition space ($x = 0 \rightarrow 1$ and $y = 0 \rightarrow 1 - x$). Surface compositions at 164 different bulk compositions were measured at 500 and 600 K. At both temperatures, Au shows the greatest tendency for segregation to the top-most surface while Pd is always depleted from the surface. Higher temperatures enhance the Au segregation. Segregation at most of the binary alloy bulk compositions matches with observations previously reported in the literature. However, surface compositions in the CuPd B2 composition region reveal segregation profiles that are nonmonotonic in bulk alloy composition. These were not observable in prior studies because of their limited resolution of composition space. An extended Langmuir−MacLean model, which describes ternary alloy segregation, has been used to analyze experimental data from the ternary alloys and to estimate pair-wise segregation free energies and segregation equilibrium constants. The ability to study surface segregation across the ternary alloy composition space with high-throughput methods has been validated, and the impact of bulk alloy phase on surface segregation is demonstrated and discussed.

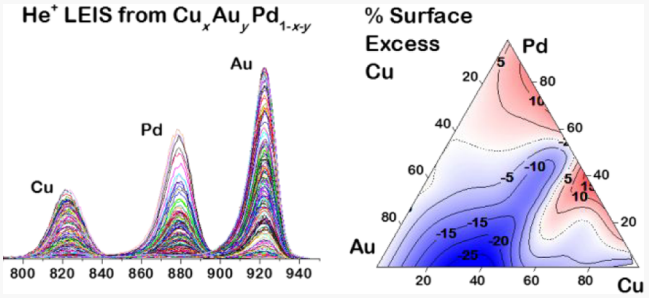

INTRODUCTION

In multicomponent materials such as alloys, surface segregation is ubiquitous, resulting in the material surface having a composition different from that of the bulk. Segregation minimizes the surface free energy and arises from differences between the component surface energies, strain energy caused by lattice mismatch of bulk components, and interactions of surface components with adsorbates. Under equilibrium conditions, the relationship between the bulk and the surface compositions is described by the Langmuir−McLean model parameterized by the Gibbs free energy of segregation. Detailed segregation models try to relate the enthalpy and entropy contributions to the free energy to bulk composition, adsorbate type, and ambient pressure.[1] As adsorption, desorption, catalytic reactions, and many other surface phenomena occur on the outer-most surface of a material, all are influenced by surface segregation. The surface composition of a multicomponent material dictates adsorption site distributions and influences surface reactions;[2] thus, understanding alloy surface segregation is critical to understanding alloy surface chemistry.

Numerous methods for determining the surface composition of a multicomponent material have been applied in studies of surface segregation. These methods can be categorized into those that are sensitive to the top-layer composition and those that measure near-surface composition. Among the top-layer composition measurement methods, scanning transmission electron microscopy (STEM) and high-resolution TEM[3] give both atom type and position with high spatial resolution. Fourier-transform infrared spectroscopy combined with CO adsorption gives vibrational spectra that can be used to quantify the coverage of those surface atom types to which CO adsorbs.[4,5] It should be noted, however, that CO adsorption can be invasive because of the different binding energies of CO to the various components of the surface and, therefore, CO may itself influence the surface composition. Xe adsorption is less invasive and combined with UV photoemission can be used to identify and quantify the surface atoms to which Xe adsorbs.[6] Perhaps, the most common method for the study of

Received: March 8, 2020
Revised: April 16, 2020
Published: April 17, 2020

https://dx.doi.org/10.1021/acs.jpcc.0c02058
J. Phys. Chem. C 2020, 124, 10605−10614

surface segregation is low-energy He^+ ion scattering (LEIS), which quantifies the top-most surface composition.[7]

For determining near-surface composition, Auger electron spectroscopy (AES), X-ray photoelectron spectroscopy (XPS), and angle-resolved XPS have been used widely. In these analysis methods, the depth resolution is dictated by the mean free paths of the photo-emitted electrons; usually ∼1 nm. Ion-sputtered depth profiling combined with LEIS or XPS is a destructive method for the study of depth-dependent composition. Secondary ion mass spectrometry with time-of-flight detection can be operated in a static mode with low detection limits.[8] Among the many techniques mentioned, LEIS developed by Brongersmal has proven to be the most effective and sensitive way of measuring top-surface compositions and thus has been widely used in surface segregation studies.[9]

To understand completely the key factors governing segregation, comprehensive study across the alloy composition space is needed; however, such studies are rare and most focus on a single alloy composition. The complicated interactions within a ternary system make it important for studies to span the entire composition space, rather than just using a few discrete compositions.[10−15] Although thermodynamic models[16−21] and computational methods[22−25] for binary alloy segregation have been developed based on numerous experimental studies under vacuum[7] and in the presence of adsorbates,[3,13,26−31] they cannot be easily extended and validated to describe segregation in ternary alloys because of a lack of experimental data.[32]

Traditional experimental and computational methods can only measure or predict segregation at one composition at a time. Thus, they are unsuitable for studies spanning the large, continuous 2D composition space of a ternary alloy. This problem is ideally suited to the development and application of a high-throughput methodology for the study of surface segregation. High-throughput experimentation has greatly accelerated material exploration over the past decade.[33−37] High-throughput experimentation allows parallel production and characterization of numerous materials with different compositions or structures. Composition spread alloy films (CSAFs) are high-throughput libraries that were first developed in the 1950s for determination of alloy phase diagrams.[38] Since then, they have been successfully applied to study the phase diagrams, electronic structures,[39] and many other properties of multicomponent alloy systems. Figure 1 illustrates a ternary CSAF prepared by deposition of three alloy components with composition gradients oriented at 120°.[40] Such CSAFs span the entirety of ternary composition space and, when analyzed using spatially resolved methods, provide much more data in one experiment than traditional methods.

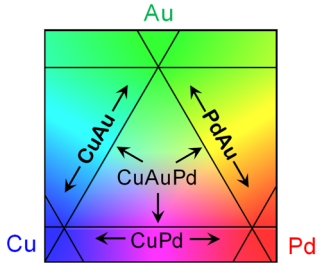

Figure 1. Schematic representation of a CSAF. Subregions of the CuAuPd ternary alloy, CuPd, AuPd, CuAu binary alloys, and pure Pd, Cu, and Au can be found on a single CSAF. The CSAF is deposited as ∼100 nm thick films on a 14 × 14 × 3 mm^3 Mo substrate.

In this work, the CuAuPd system was chosen for the ternary segregation study because it is a well-studied alloy system with a known phase diagram[39] and components with very different masses, allowing easy quantification of surface composition using LEIS. Pd alloys catalyze many hydrogenation[41,42] and oxidization[5,43] reactions and can be used as hydrogen purification membranes.[12,44−54] Segregation in PdAu,[1,22,52,55−60] PdCu,[7,25,27,28,61] and CuAu[62,63] binary alloys has been described frequently in the literature, and CuAuPd segregation has also been reported at a few discrete compositions.[10,12] It is known that under vacuum conditions, Au and Cu in Pd alloys are the surface-enriched elements. Their segregation minimizes system energy by reducing the strain energy of the bulk lattice and by covering the surface with low-surface energy alloy components. The phase diagram of CuAuPd has also been studied.[39,53,64−66] Although all three pure components have face-centered cubic bulk structures, the Cu_xPd_{1-x} binary alloy exhibits a B2 phase over the composition range $x = 0.45 \rightarrow 0.65$. The B2 phase has a CsCl structure with an ordered body-centered cubic (bcc) lattice. In the ternary $Cu_xAu_yPd_{1-x-y}$ alloy, this B2 phase extends to an Au composition of $y \approx 0.20$. This ordered B2 phase is stable at low temperature and shows superior H_2 permeability and considerable tolerance to impurities such as H_2S in H_2-containing gas streams.[67,68] Because of its industrial relevance and ease of characterization, CuAuPd is an ideal system for ternary alloy segregation study.

In this work, surface segregation in CuAuPd under ultrahigh vacuum (UHV) conditions was measured at 500 and 600 K at 164 different bulk compositions on a $Cu_xAu_yPd_{1-x-y}$ CSAF spanning ternary composition space, $x = 0 \rightarrow 1$ and $y = 0 \rightarrow 1 - x$. The existence of the B2 phase was identified by the LEIS signal intensity, and the influence of the B2 phase on surface segregation has been observed experimentally. Segregation along the three binary alloy compositions matches that reported in earlier studies. Measurements of surface segregation have also been made spanning the ternary composition space, and the free energies of segregation were estimated using a Langmuir−McLean model extended for application to ternary systems.[32]

EXPERIMENTAL SECTION

CSAF Fabrication. $Cu_xAu_yPd_{1-x-y}$ CSAFs were deposited under UHV conditions by combining physical vapor deposition sources with rotatable shadow masks, as described elsewhere.[40] A polycrystalline Mo block (14 × 14 × 3 mm) was used as the substrate to minimize alloying with CSAF components during annealing, and no sign of Mo was detected at the alloy surface during the course of these measurements. Ta heating wires and a type K thermocouple were spot-welded onto the edge of the substrate to allow heating and control of the substrate temperature. In the UHV deposition chamber, cycles of Ar^+ sputtering and annealing were performed to clean the Mo substrate before physical vapor deposition of the CSAF. Deposition rates for all three sources were ∼11 nm/h and were recalibrated every 2 h using a quartz crystal microbalance. The deposition period lasted 8 h at a base pressure of 1×10^{-9} Torr and a substrate temperature of ∼300 K. After deposition, the CSAF was annealed at 800 K in UHV for 1 h before cooling to room temperature, yielding a ∼100 nm polycrystalline thin film.[66]

https://dx.doi.org/10.1021/acs.jpcc.0c02058
J. Phys. Chem. C 2020, 124, 10605−10614

Bulk Characterization—Energy-Dispersive X-ray. Energy-dispersive X-ray spectroscopy (EDX) was used to map the CSAF bulk composition on a 27 × 27 grid of points spaced 0.5 mm apart (Figure 2, gray ■). EDX spectra were obtained

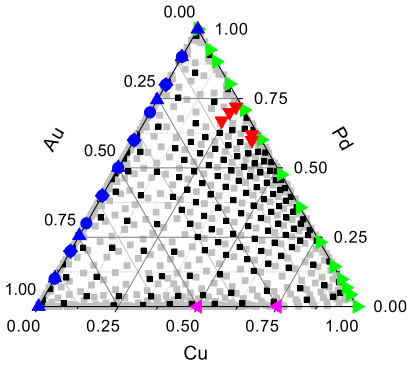

Figure 2. Ternary composition diagram indicating the bulk compositions determined by EDX (gray ■). LEIS spectra were collected at selected bulk compositions (black ■). Surface compositions examined in published LEIS studies by various authors are labeled in color: blue Swartzfager[60] (blue, ▲), Yi[59] (blue, ◆), and Boes[22] (blue ●) measurements on PdAu. In green, Priyadarshini[7] (green, ▶) measurements on CuPd. In purple, Beikler[69] and Taglauer[69,70] (purple, ◀) measurements on CuAu. In red, Miller[10] (red, ▼) measurements on CuAuPd.

using a TESCAN Vega3 LM SEM equipped with an Oxford Inca Energy 350 X-ray detector. At each point, the spectrum was obtained by rastering a 20 keV electron beam across a 50 × 50 μm^2 area. The beam intensity and live time were adjusted to give a dead time fraction of ∼30% during spectrum acquisition, yielding a desirable signal-to-noise ratio. EDX spectra were analyzed using the *Thinfilm ID* software using the Pd L-, Cu K- and L-, and Au L- and M-series lines to quantify bulk composition and the thickness of the thin film at each point. Repeated scans over the same points give an uncertainty of <1 nm in each component thickness. Composition−position maps across the CSAF were thereby determined.

Surface Characterization—LEIS. He^+ LEIS was performed in ThetaProbe to determine the top-surface compositions of the CSAF. Helium was leaked into the UHV chamber at a pressure of 1.0 × 10^{-8} Torr and was ionized to have an initial kinetic energy of E_0 = 1 keV. A 500 μm diameter spot was created by He^+ ions impinging at 50° from the surface normal, and the scattered ions were collected at an angle of 24° from the surface normal. Using an ion current of ∼50 nA, three scans of 50 s each were used to collect the LEIS spectra at each of the 164 points spaced by ∼500 μm. These conditions minimized CSAF damage while yielding high signal-to-noise level. Three points on the CSAF contain pure components, as measured by EDX. The LEIS peak areas at E/E_0 = 0.82 (Cu), E/E_0 = 0.88 (Pd), and E/E_0 = 0.92 (Au) and the areas of the peaks obtained from the pure component points have been used for quantification of the surface composition at each point across the CSAF (Figure 2, black ■), as will be shown in the section on Surface Composition Mapping.

Segregation Measurements. After acquiring EDX spectra to map the bulk composition, the CuAuPd CSAF was transferred into ThetaProbe to map the surface composition using LEIS. First, the CSAF was cleaned at each of 164 points for 5 h in total at 300 K using 1 keV He^+ sputtering and then annealed at 800 K to restore the surface structure. Surface cleanliness was checked using the C 1s XPS signal. Then, the CSAF was cooled from 800 K to the desired measurement temperature (500 or 600 K) and held for over 1 h before acquiring LEIS spectra at the selected 164 points that span ternary composition space (Figure 2, black ■). LEIS spectra at $T \leq 400$ K show low ion yields at the pure-component points, especially at pure Pd and Cu points, which indicates possible contamination of the surface by H, CO, or CO_2 adsorption from the background. Direct evidence for surface contamination was not found because of the limited LEIS energy-collection window used.

■ RESULTS

Bulk Composition Mapping. EDX has been used to map the bulk composition of the $Cu_xAu_yPd_{1-x-y}$ CSAF across a 27 × 27 grid of points spaced by 0.5 mm. This map was used to select 164 points spanning the ternary composition region for analysis of surface segregation using LEIS (Figure 2, black ■). Over most of the CSAF, the analysis points are spaced to give ∼10% composition resolution. Over the region of the ternary space in which the B2 phase is expected, the analysis points are spaced to yield ∼5% composition resolution. Also, Figure 2 shows the bulk compositions at which previous quantitative LEIS measurements of segregation have been made and reported.[7,10,22,59,60,69,70] These are bulk compositions along each binary axis (blue, green, and purple symbols) and in a small region of ternary alloy compositions (solid red downward triangles). Figure 2 demonstrates that this study

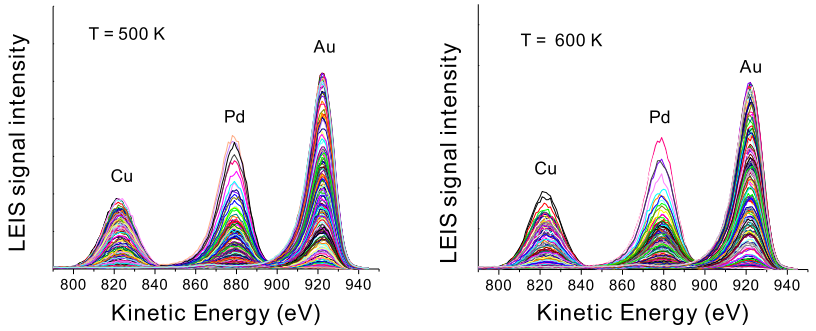

Figure 3. He^+ LEIS spectra at 164 bulk $Cu_xAu_yPd_{1-x-y}$ alloy compositions obtained at 500 (left) and 600 K (right); (He^+ E_0 = 1 keV; scattering angle = 103°; scan time = 150 s; He^+ beam diameter = 500 μm). The Cu, Pd, and Au peaks are well-resolved, and their peak energies, E/E_0, match the predictions of the binary collision model.

https://dx.doi.org/10.1021/acs.jpcc.0c02058
J. Phys. Chem. C 2020, 124, 10605−10614

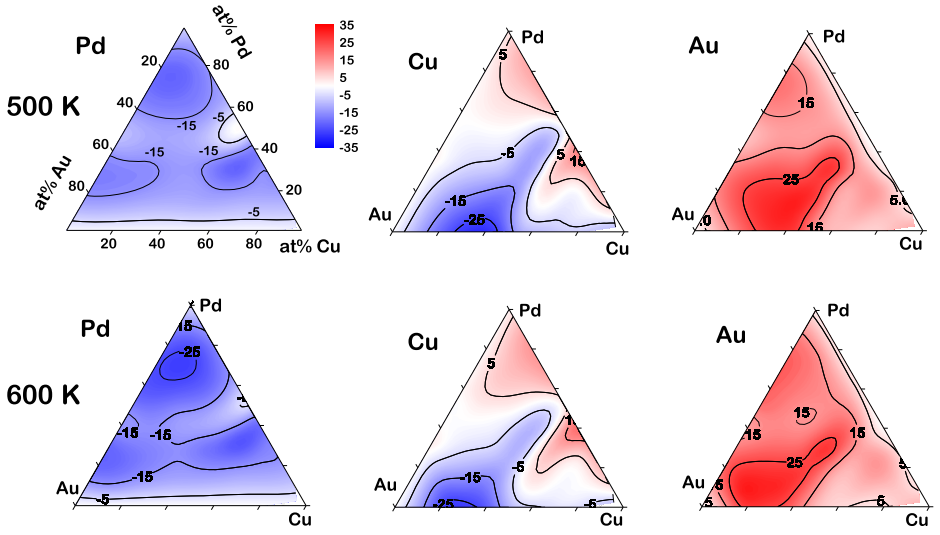

Figure 4. Ternary diagrams showing excess surface concentrations of Pd, Cu, and Au, defined by eqs 2a–2c. Data were obtained at 500 (first row) and 600 K (second row). The blue regions on the Cu and Pd maps indicate lower surface coverage of Cu and Pd than in the bulk, and the red regions on the Au maps indicate the Au-enriched top surface; Cu is enriched on the surface only at low Au compositions.

of ternary alloy segregation is far more comprehensive than any prior study of the $Cu_xAu_yPd_{1-x-y}$ system and, to the best of our knowledge, any other ternary alloy.

Surface Composition Mapping. Spatially resolved He^+ LEIS was used to map the top-most layer surface composition of the $Cu_xAu_yPd_{1-x-y}$ CSAF across the bulk composition space. Figure 3 shows the LEIS spectra obtained at 164 different bulk compositions at temperatures of 500 and 600 K. The contributions from each element are easily resolved in each of the spectra because their atomic masses are significantly different: m_{Cu} = 63.5, m_{Pd} = 106.4, and m_{Au} = 197.0. The peak energies for the three alloy components fall at $E_{Cu} = 0.82 \times E_0$, $E_{Pd} = 0.88 \times E_0$, and $E_{Au} = 0.92 \times E_0$, consistent with the scattering geometry and the prediction of the binary collision model.[71] Spectra at 300 and 400 K show relatively low Cu and Pd intensities even at pure component points and some attenuation of the Au signal. We believe that this arises from adsorption of background gasses onto the alloy surface, thereby screening some fraction of the surface atoms. During temperature-programmed desorption experiments, the peak desorption temperature for CO on Pd is $T_p \cong 500$ K, and the pressure–temperature phase diagram for CO adsorption on Pd shows that at a pressure of 10^{-9} Torr, CO is completely desorbed at $T \geq 500$ K.[72] The desorption temperatures of most other UHV background gasses from any of the three alloy components are typically lower than this, so it is reasonable to expect that at $T \geq 500$ K, the surface should remain contaminant free. Further analysis has been limited to the spectra obtained at 500 and 600 K.

Given the He^+ scattering intensity from the clean surfaces of the three pure components of the $Cu_xAu_yPd_{1-x-y}$ alloy, it is possible to estimate the surface composition at any bulk composition (x, y) at which LEIS spectra have been obtained. The following equation has been used to determine the top surface atom fraction of Pd at each bulk composition

$$\theta_{Pd}^{top}(x,y) = \frac{\frac{I_{Pd}(x,y)}{I_{Pd}^{\circ}}}{\left[\frac{I_{Pd}(x,y)}{I_{Pd}^{\circ}}\right] + \frac{\rho_{Cu}^{\circ}}{\rho_{Pd}^{\circ}}\left[\frac{I_{Cu}(x,y)}{I_{Cu}^{\circ}}\right] + \frac{\rho_{Au}^{\circ}}{\rho_{Pd}^{\circ}}\left[\frac{I_{Au}(x,y)}{I_{Au}^{\circ}}\right]} \quad (1)$$

where I_{Pd} represents the area of the Pd LEIS peak after linear background subtraction and Gaussian–Lorentzian sum peak fitting. The quantities I_{Pd}°, I_{Cu}°, and I_{Au}° are the measured LEIS peak areas of the pure components, and ρ_{Pd}°, ρ_{Cu}°, and ρ_{Au}° are the areal surface atom densities of the three pure components estimated from the bulk primitive lattice constant, a^2. The factors $\rho_{Cu}^{\circ}/\rho_{Pd}^{\circ}$ and $\rho_{Au}^{\circ}/\rho_{Pd}^{\circ}$ account for the differences in surface atom densities between pure components. The three pure component materials all have face-centered cubic (fcc) bulk structures with lattice parameters of a_{Pd} = 0.386 nm, a_{Cu} = 0.360 nm, and a_{Au} = 0.406 nm. Based on their lattice constants, $\rho_{Cu}^{\circ}/\rho_{Pd}^{\circ}$ and $\rho_{Au}^{\circ}/\rho_{Pd}^{\circ}$ are estimated to be 1.150 and 0.904, respectively. Expressions for alloy surface coverages without these additional factors will lead to overestimation of the surface concentrations of components that have larger lattice constants and underestimation for those with smaller lattice constants. Equations analogous to eq 1 have been used to quantify the surface coverages of Cu, θ_{Cu}^{top}, and Au, θ_{Au}^{top}, in the $Cu_xAu_yPd_{1-x-y}$ alloy.

To visualize the segregation data over the ternary composition space, maps of excess surface concentration (in units of atomic percent), defined as

$$\Delta\theta_{Cu}(x,y) = \theta_{Cu}^{top}(x,y) - x \quad (2a)$$

$$\Delta\theta_{Au}(x,y) = \theta_{Au}^{top}(x,y) - y \quad (2b)$$

$$\Delta\theta_{Pd}(x,y) = \theta_{Pd}^{top}(x,y) - (1 - x - y) \quad (2c)$$

are shown in Figure 4. Red indicates surface segregation while blue indicates surface depletion. The color maps reveal significant Au segregation and Pd depletion at all compositions. Cu is enriched relative to Pd in regions where the Au concentration is low. In the case of Au, segregation reaches as much as $\Delta\theta_{Au}(x,y) \cong 30\%$ at high bulk Au compositions. The maximum depletion of Pd occurs at three regions of the bulk composition and reaches $\Delta\theta_{Pd}(x,y) \cong -25\%$. The final observation is that while the segregation profiles along the CuAu and the AuPd binaries are fairly smooth and always positive or always negative, the segregation profile along the CuPd binary is more complex. It goes through an inversion in

https://dx.doi.org/10.1021/acs.jpcc.0c02058
J. Phys. Chem. C 2020, 124, 10605–10614

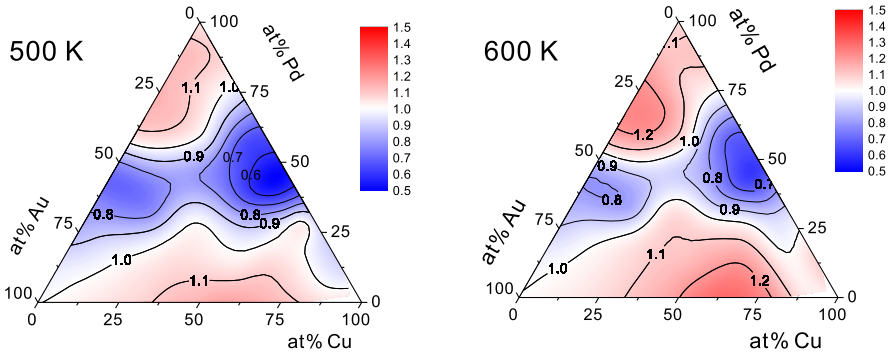

Figure 5. Ternary diagrams showing the fractional excess surface atom density, $f_\rho(x, y)$, defined by eq 7. Data were obtained at 500 (left) and 600 K (right). The blue region centered at $Cu_{0.5}Pd_{0.5}$ shows notably lower (~50%) surface atom density than expected, indicating the presence of the B2 structure.

the region around $x = 0.5$, where the B2 phase is observed, clearly demonstrating that the bulk crystal structure has an influence on surface segregation.

DISCUSSION

LEIS Signal Intensity Map. Ignoring matrix effects, the LEIS intensity (peak area) from each component should be proportional to its areal surface atom density, ρ_i

$$I_{Pd}(x, y) = I_{Pd}^{\circ}\frac{\rho_{Pd}(x, y)}{\rho_{Pd}^{\circ}} \tag{3}$$

where I_{Pd}° and ρ_{Pd}° are the LEIS intensity and surface atom density of a clean, pure Pd surface, respectively. The surface atomic fraction can be expressed as

$$\theta_{Pd}^{top}(x, y) = \frac{\rho_{Pd}(x, y)}{\rho_{tot}(x, y)} = \frac{\rho_{Pd}(x, y)}{\rho_{Cu}(x, y) + \rho_{Au}(x, y) + \rho_{Pd}(x, y)} \tag{4}$$

Substituting eq 3 into eq 4 gives

$$\theta_{Pd}^{top}(x, y) = \frac{\rho_{Pd}^{\circ}\frac{I_{Pd}(x,y)}{I_{Pd}^{\circ}}}{\rho_{Cu}^{\circ}\frac{I_{Cu}(x,y)}{I_{Cu}^{\circ}} + \rho_{Au}^{\circ}\frac{I_{Au}(x,y)}{I_{Au}^{\circ}} + \rho_{Pd}^{\circ}\frac{I_{Pd}(x,y)}{I_{Pd}^{\circ}}} \tag{5}$$

The value of $\rho_{tot}(x, y) = \rho_{Cu}(x, y) + \rho_{Au}(x, y) + \rho_{Pd}(x, y)$ used in eq 4 can be estimated using Vegard's law and the lattice constants of the three pure components.

The surface atom density at any given bulk composition, (x, y), can be estimated from the measured LEIS signals.

$$\rho_{tot}(x, y) = \frac{\rho_{Cu}^{\circ}}{I_{Cu}^{\circ}}\cdot I_{Cu}(x, y) + \frac{\rho_{Au}^{\circ}}{I_{Au}^{\circ}}\cdot I_{Au}(x, y) + \frac{\rho_{Pd}^{\circ}}{I_{Pd}^{\circ}}\cdot I_{Pd}(x, y) \tag{6}$$

This can be compared with the expected value of the surface atom density based on the primitive lattice constant, a, predicted from Vegard's law, $\rho_V = a^{-2/3}$, at each alloy composition. The fractional surface atom density observed relative to that expected from the fcc bulk structure of the three pure components is now defined as

$$f_\rho(x, y) = \frac{\rho_{tot}(x, y)}{\rho_V(x, y)} \tag{7}$$

If f_ρ deviates significantly from unity, then another crystal structure might be present. The LEIS surface density maps are shown in Figure 5. Two blue regions with significantly low values of I_{tot} can be identified from the LEIS total intensity map. The darker one centered at $Cu_{0.5}Pd_{0.5}$ shows 50% lower LEIS intensity than expected from the pure components, indicating a crystal structure of lower surface atom density, consistent with the existence of the B2 phase in the CuAuPd phase diagram.[39]

Ternary Alloy Segregation Equilibrium. The Langmuir−McLean equation has been widely used to describe equilibrium surface segregation in binary alloys.[27] The Langmuir−McLean model describes a system in which different metal atoms can swap their positions between the bulk and the surface, and the alloy maintains a constant number of available surface sites during segregation.[73] For a two-component equilibrium describing segregation in AuPd

$$\frac{\theta_{Au}}{\theta_{Pd}} = K_{AuPd}\frac{x_{Au}}{x_{Pd}} = \frac{x_{Au}}{x_{Pd}}\cdot\exp\left(\frac{-\Delta G_{AuPd}}{RT}\right) \tag{8}$$

where θ_i represents the fractional surface composition of component i, and x_i represents its fractional contribution to the bulk composition. This is equivalent to

$$\theta_{Au} = \frac{K_{AuPd}x_{Au}}{x_{Pd} + K_{AuPd}x_{Au}} \tag{9a}$$

$$\theta_{Pd} = \frac{x_{Pd}}{x_{Pd} + K_{AuPd}x_{Au}} \tag{9b}$$

where K_{AuPd} is the equilibrium constant describing the following atom-exchange reaction

$$Au^{bulk} + Pd^{surf} \rightleftharpoons Au^{surf} + Pd^{bulk} \tag{10}$$

A negative value of the segregation free energy, ΔG_{AuPd}, implies excess Au at the surface, that is, $\theta_{Au} > x_{Au}$.

Segregation in the $Cu_xAu_yPd_{1-x-y}$ ternary system can be described using three two-atom exchange reactions and their corresponding equilibrium constants

$$Au^{bulk} + Pd^{surf} \rightleftharpoons Au^{surf} + Pd^{bulk} \qquad K_{AuPd} = \frac{\theta_{Au}x_{Pd}}{x_{Au}\theta_{Pd}} \tag{11a}$$

https://dx.doi.org/10.1021/acs.jpcc.0c02058
J. Phys. Chem. C 2020, 124, 10605−10614

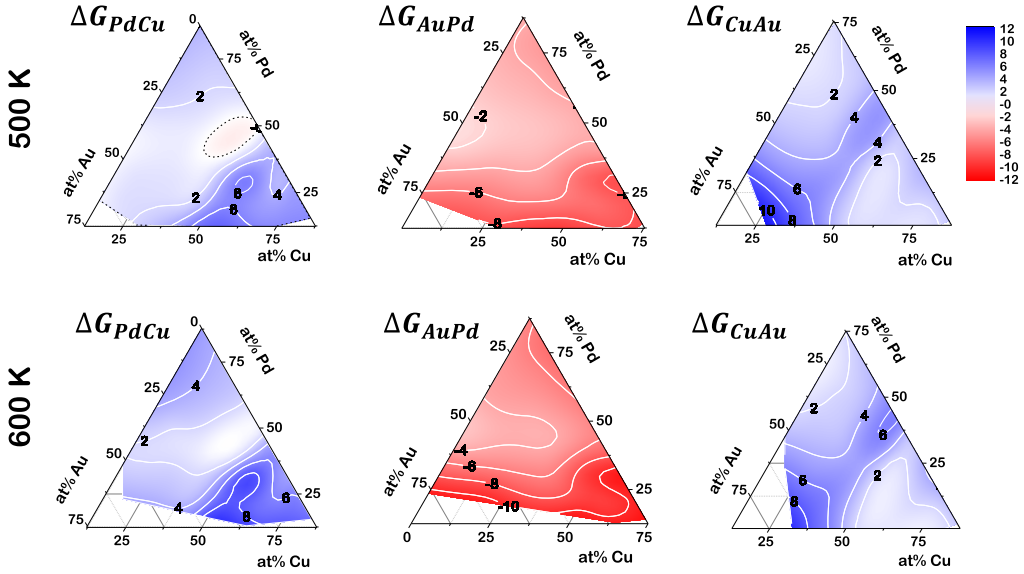

Figure 6. Ternary diagrams showing pair-wise segregation Gibbs free energies defined by eq 13. Data were obtained at 500 (first row) and 600 K (second row), and figures from left to right are ΔG_{PdCu}, ΔG_{AuPd}, and ΔG_{CuAu} in units of kJ/mol. Pair-wise segregation free energies <10 kJ/mol are observed in these experiments.

$$Pd^{bulk} + Cu^{surf} \rightleftharpoons Pd^{surf} + Cu^{bulk} \qquad K_{PdCu} = \frac{\theta_{Pd} x_{Cu}}{x_{Pd} \theta_{Cu}} \tag{11b}$$

$$Cu^{bulk} + Au^{surf} \rightleftharpoons Cu^{surf} + Au^{bulk} \qquad K_{CuAu} = \frac{\theta_{Cu} x_{Au}}{x_{Cu} \theta_{Au}} \tag{11c}$$

These represent only two independent systems in equilibrium because $K_{AuPd}K_{PdCu}K_{CuAu} = 1$, or equivalently, $\Delta G_{AuPd} + \Delta G_{PdCu} + \Delta G_{CuAu} = 0$. Note that these definitions imply that in the case $K_{CuAu} > 1$ (or $\Delta G_{CuAu} < 0$), the first component, Cu, segregates preferentially over the second, Au.

The surface compositions can be expressed as functions of bulk composition and the equilibrium constants

$$\theta_{Pd} = \frac{x_{Pd}}{x_{Pd} + K_{PdCu}^{-1} x_{Cu} + K_{AuPd} x_{Au}} \tag{12a}$$

$$\theta_{Cu} = \frac{K_{PdCu}^{-1} x_{Cu}}{x_{Pd} + K_{PdCu}^{-1} x_{Cu} + K_{AuPd} x_{Au}} \tag{12b}$$

$$\theta_{Au} = \frac{K_{AuPd} x_{Au}}{x_{Pd} + K_{PdCu}^{-1} x_{Cu} + K_{AuPd} x_{Au}} \tag{12c}$$

In this work, bulk compositions, x_i, were measured by EDX, and surface compositions, θ_i, were determined by LEIS. For segregation at 500 K and at 600 K, values of K_{PdCu} and K_{AuPd} were calculated from experimental data spanning the bulk composition space and converted to Gibbs free energy changes (Figure 6) using eq 13. Because pair-wise equilibrium constants, K_{AB}, are defined by ratios, only data points where both terms in denominators (bulk concentration of the first component, A, and surface concentration of the second component, B) are >2% have been taken into account in free energy estimation.

$$\Delta G_{AB} = -RT \cdot \ln K_{AB} \tag{13}$$

The data in Figure 6 make it clear that the segregation of Au with respect to Pd is spontaneous, $\Delta G_{AuPd} < 0$, at all bulk alloy compositions. Similarly, the segregation of Au with respect to Cu is also spontaneous, $\Delta G_{AuCu} = -\Delta G_{CuAu} < 0$. In the equilibrium defining segregation of Cu and Pd, Cu segregation is thermodynamically spontaneous, other than in the region with $x_{Cu} \cong x_{Pd}$ and $x_{Au} < 0.2$, in which the B2 phase is formed and $\Delta G_{PdCu} \cong 0$. This result is not surprising given that the B2 phase of $Cu_{0.5}Pd_{0.5}$ has an ordered CsCl structure, implying that there is a net free energy penalty for the configurational disorder that would accompany segregation of either component.

Segregation in Binary Cu−Au−Pd Alloys. The segregation data shown for $Cu_xAu_yPd_{1-x-y}$ in Figure 4 are, to the best of our knowledge, the most comprehensive data set yet obtained for a ternary system and there is little other data for comparison. However, because we are able to make CSAFs that truly span composition space, we have also been able to study segregation in the three binary alloy combinations available to us. These data are compared below to those obtained during other studies of the same binary alloys. Among other things, these comparisons demonstrate the ability of the CSAF library to reproduce previously observed segregation behavior.

Segregation in PdAu Alloys. PdAu segregation has been discussed in many studies with the common conclusion that Au segregates to the surface preferentially.[1,22,52,55−60] Pd and Au both have fcc structures as pure components (see PdAu phase diagram in Supporting Information 1). Because of the small lattice mismatch (4.8%) between Pd and Au and their negative enthalpy of mixing,[74,75] PdAu alloys also have an fcc structure at all compositions. Ordered phases centered at Pd_3Au and $PdAu_3$ are shown to be stable to high temperatures (<1100 K), and there is an ordered PdAu phase that is predicted to be stable at $T < 373$ K.[75]

Among the 164 different $Cu_xAu_yPd_{1-x-y}$ bulk compositions characterized in this study, there are 20 compositions with bulk Cu concentrations of <2 at. %, which is close to the uncertainty limit of EDX analysis. To compare the segregation data for these alloy compositions with those from prior PdAu binary alloy studies, the bulk and surface compositions of these 20

https://dx.doi.org/10.1021/acs.jpcc.0c02058
J. Phys. Chem. C 2020, 124, 10605−10614

points are normalized to consider only their Pd and Au relative concentrations and plotted in Figure 7.

$$\bar{x}_{Au} = \frac{x_{Au}}{x_{Pd} + x_{Au}} \quad (14a)$$

$$\bar{\theta}_{Au} = \frac{\theta_{Au}}{\theta_{Pd} + \theta_{Au}} \quad (14b)$$

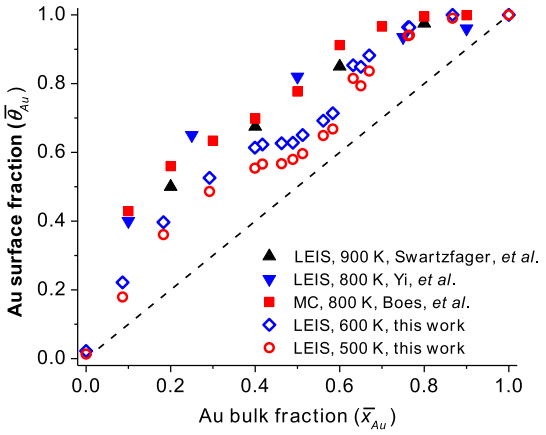

Figure 7. PdAu segregation profiles at 500 and 600 K (open symbols) compared with data from Swartzfager,[62] Yi,[61] and Boes.[17] Au segregation is enhanced at higher temperatures. The segregation profiles all show deviation from the convex to concave curvature at a bulk Au fraction of $\bar{x}_{Au} = 0.5$.

Figure 7 compares the normalized surface Au fractions, $\bar{\theta}_{Au}$, as a function of normalized bulk Au fraction, $\bar{x}_{Au}$, at 500 and 600 K for all 20 binary compositions on the CSAF, with the results of three other LEIS and Monte Carlo studies. The segregation profiles at 500 and 600 K show shapes similar to those observed in other studies, with Au being enriched at the surface at all bulk compositions and greater Au surface segregation at higher temperatures.

In all studies shown in Figure 7, a concave curvature in the segregation profile can be observed at a bulk composition of roughly $Pd_{0.5}Au_{0.5}$. The reason for the concave curvature is not well understood. As no electron backscatter diffraction pattern was taken on the CSAF studied, we cannot exclude the possibility that an ordered structure,[75] which may contribute to the curvature, forms near equiatomic composition. The relatively low LEIS intensity in this composition region, $x_{Au} = 0.4 \rightarrow 0.6$, in Figure 5 also supports the existence of a non-fcc(111) atomic structure. According to the PdAu phase diagram,[75] Au_3Pd and $AuPd_3$ have ordered $L1_2$ structures at $T < 1100$ K. Although some ordered structures for equimolar compositions have been proposed on the basis of ab initio calculations, they have not been identified experimentally.[74] The effect of crystal structure on segregation will be discussed further in the following section.

Segregation in PdCu Alloys. PdCu alloys have been extensively explored as materials for H_2 separation membranes because of their high H_2 permeability and low cost.[50,53] The existence of a B2 phase at roughly equimolar bulk composition in the PdCu phase diagram is well known (see Supporting Information 2).[65] The B2 phase is an ordered CsCl structure on a bcc lattice. This B2 phase has been identified in CSAFs using both electron backscatter diffraction and careful measurements of Cu $2p_{3/2}$ core level shifts observed using XPS.[39,66,76,77] In this work, we find that Cu segregation to the surface is inhibited over a composition range that is roughly aligned with that of the B2 phase. Figure 8 shows that there is a narrow bulk composition region, $0.45 < x_{Cu} < 0.55$, over which the surface excess of Cu drops to almost zero.

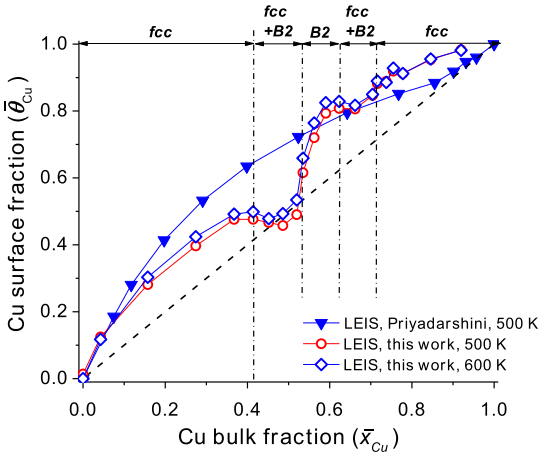

Figure 8. Comparison of PdCu segregation profile at 500 K with similar data in the literature.[7] Obvious deviations occur over the $\bar{x}_{Cu}$ range 40–60%, which reveals a suppression of the Cu segregation relative to alloys outside this range. Composition boundaries of fcc, B2, and transition regions from the literature are labeled with dotted lines. An offset of ~4 at. % in the B2 phase region is observed between the current work and literature.

Many surface segregation studies on PdCu have been published,[7,25,27,28,31,61,78−80] mostly on discrete composition samples,[28,78−80] in the presence of adsorbates,[27,28] or studied by surface analysis methods that are not as accurate as LEIS.[31] Only Priyadarshini's work,[7] whose measurements were also done on a CSAF with a continuous composition spread and under UHV conditions, will be compared with data from the current work. Points on the CSAF with bulk Au atomic concentrations <2% (within EDX uncertainty) have been normalized to describe only their Pd−Cu binary compositions, and the corresponding segregation profiles at 500 and 600 K are shown in Figure 8 and compared to that of Priyadarshini et al.[7] Compositions outside the B2 region agree fairly well with earlier results while an obvious deviation can be seen within the B2 region, where Cu shows little tendency to segregate.

Several differences between the experimental setup and treatment of the CSAFs in Priyadarshini's work and this experiment may have contributed to the fact that the effect of the B2 phase was not observed earlier. A single-crystal Mo(110) substrate was used in Priyadarshini's work, which may lead to preferential ordering of grain orientations while a polycrystalline Mo substrate was used in this study. The previous work also took only two measurements across the composition region of the B2 phase. Perhaps, the most critical difference between the two experiments is the fact that in Priyadarshini's experiments, the sample was cooled actively using liquid nitrogen, allowing much more rapid cooling from the annealing temperature to the measurement temperature. Prior work has shown that rapid cooling can freeze the CuPd alloy into the high-temperature fcc phase at all compositions.[79,81] This would be sufficient for the B2 phase to have been missed in the earlier segregation study.

https://dx.doi.org/10.1021/acs.jpcc.0c02058
J. Phys. Chem. C 2020, 124, 10605−10614

We observe a decrease in the Cu segregation over the composition range of the B2 phase existence (Figure 8) to the point that there is no excess surface Cu at bulk Cu compositions in the range $0.45 < x_{Cu} < 0.52$. The origin of the apparent discontinuity in the Cu segregation profile over the composition range associated with the B2 phase may be the fact that the B2 phase is an ordered alloy (CsCl structure on a bcc lattice) while the fcc phase is disordered. The ordered bulk structure implies that enthalpy has dominated over the configurational entropy of the disorder fcc structure. Presumably, this also inhibits exchange of Cu atoms from the bulk B2 structure with surface Pd atoms. Verifying this would require computational simulation of segregation in the CuPd system.[25]

Segregation in AuCu Alloys. At $T > 700$ K, Au_xCu_{1-x} alloys at all compositions form random solid solutions on an fcc lattice (see Supporting Information 3).[82] Cooling to $T < 500$ K results in the formation of three-ordered phases with nominal stoichiometries Cu_3Au, CuAu, and $CuAu_3$. At 600 K, one has order phases over the range $0.2 < x_{Au} < 0.65$. Special attention has been paid to Cu_3Au because of its surface-ordering properties.[83] As a result of strong ordering tendency, $Cu_3Au(100)$ exhibits almost ideal termination at $T < 663$ K[63] (order−disorder transition temperature) with a top layer Au composition of $\theta_{Au} = 0.5$ and a second layer Au composition of $\theta_{Au}^{2nd} = 0$. On $Cu_3Au(110)$, some intermixing was observed[84] between first and second atomic layers and $\theta_{Au} \approx 0.4$ at around 500−600 K. A low-energy electron diffraction study[85] shows no segregation of Au on the $Cu_3Au(111)$ surface. On CuAu(100), a top-most layer Au composition of $\theta_{Au} = 0.93$ was measured by LEIS at 400−700 K.[69,70]

Figure 9 shows segregation profiles obtained in this work at 500 and 600 K, revealing excess Au at all surface compositions

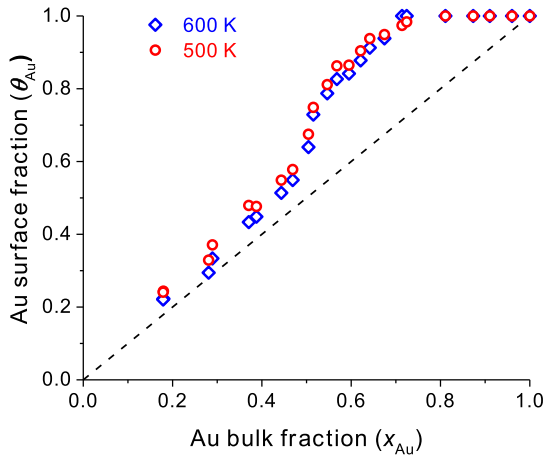

Figure 9. Segregation of Au in Au_xCu_{1-x} at 500 and 600 K. Segregation does not show temperature dependence over the measured range. The excess surface coverage of Au is higher over the Au-rich composition range than over the Cu-rich range. The top surface composition is ∼100% Au when the bulk Au concentration is >70 at. %.

and low temperature dependence. However, it is quite clear that the degree of surface segregation over the bulk Au composition range $0.2 < x_{Au} < 0.5$ is relatively low. In contrast, for bulk Au compositions $x_{Au} > 0.5$, the degree of surface segregation increases dramatically to the point that for $x_{Au} > 0.7$, the top-most surface has $\theta_{Au} \approx 1$. This is consistent with observations from the literature,[85] in which stronger Au segregation was observed at $x_{Au} = 0.75$ than that at $x_{Au} = 0.25$ by AES.

CONCLUSIONS

In this work, a $Cu_xAu_yPd_{1-x-y}$ CSAF has been shown to serve as a valuable material library for the high-throughput study of surface segregation using He^+ LEIS across the composition space. It is important to note that while the $Cu_xAu_yPd_{1-x-y}$ CSAF has the virtue of allowing study of all alloy compositions in the ternary space, it is not a single crystal with well-defined surface orientation. Rather it is representative of a polycrystalline alloy material.

The major findings of this work are summarized as follows:

(1) Au preferentially segregates to the top surface of $Cu_xAu_yPd_{1-x-y}$; Pd is depleted from the top surface at all bulk compositions; and Cu is only enriched in the top surface at low Au concentrations.

(2) Suppression of segregation seems to be correlated to the existence of ordered phases in the alloy bulk. This can be rationalized by the enthalpy penalty associated with the disorder introduced into the bulk structure by segregation of one component to the surface.

ASSOCIATED CONTENT

Supporting Information

The Supporting Information is available free of charge at https://pubs.acs.org/doi/10.1021/acs.jpcc.0c02058.

Links to the binary phase diagrams for AuPd, CuPd, and CuAu (PDF)

AUTHOR INFORMATION

Corresponding Author

Andrew J. Gellman − *Department of Chemical Engineering and W. E. Scott Institute for Energy Innovation, Carnegie Mellon University, Pittsburgh, Pennsylvania 15213, United States;* orcid.org/0000-0001-6618-7427; Phone: 412-268-3848; Email: gellman@cmu.edu

Authors

Chunrong Yin − *Department of Chemical Engineering, Carnegie Mellon University, Pittsburgh, Pennsylvania 15213, United States*

Zhitao Guo − *Department of Chemical Engineering, Carnegie Mellon University, Pittsburgh, Pennsylvania 15213, United States*

Complete contact information is available at: https://pubs.acs.org/10.1021/acs.jpcc.0c02058

Notes

The authors declare no competing financial interest.

ACKNOWLEDGMENTS

Initial collection of the data presented herein was conducted with support from NSF-CHE1566228. Final data analysis and manuscript preparation have been conducted with support from NSF CBET1921946.

REFERENCES

(1) Li, Z.; Furlong, O.; Calaza, F.; Burkholder, L.; Poon, H. C.; Saldin, D.; Tysoe, W. T. Surface Segregation of Gold for Au/Pd(111)

Alloys Measured by Low-Energy Electron Diffraction and Low-Energy Ion Scattering. *Surf. Sci.* **2008**, *602*, 1084−1091.
(2) Ruban, A. V.; Skriver, H. L.; Nørskov, J. K. Surface Segregation Energies in Transition-Metal Alloys. *Phys. Rev. B: Condens. Matter Mater. Phys.* **1999**, *59*, 15990−16000.
(3) Zou, L.; Li, J.; Zakharov, D.; Saidi, W. A.; Stach, E. A.; Zhou, G. Atomically Visualizing Elemental Segregation-Induced Surface Alloying and Restructuring. *J. Phys. Chem. Lett.* **2017**, *8*, 6035−6040.
(4) Beermann, V.; Gocyla, M.; Kühl, S.; Padgett, E.; Schmies, H.; Goerlin, M.; Erini, N.; Shviro, M.; Heggen, M.; Dunin-Borkowski, R. E.; et al. Tuning the Electrocatalytic Oxygen Reduction Reaction Activity and Stability of Shape-Controlled Pt-Ni Nanoparticles by Thermal Annealing -Elucidating the Surface Atomic Structural and Compositional Changes. *J. Am. Chem. Soc.* **2017**, *139*, 16536−16547.
(5) Gao, F.; Wang, Y.; Goodman, D. W. CO Oxidation over AuPd(100) from Ultrahigh Vacuum to near-Atmospheric Pressures: The Critical Role of Contiguous Pd Atoms. *J. Am. Chem. Soc.* **2009**, *131*, 5734−5735.
(6) Küppers, J.; Michel, H.; Nitschké, F.; Wandelt, K.; Ertl, G. Xenon Adsorption as a Tool for Local Surface Structure Determination at Ir(100) Surfaces. *Surf. Sci.* **1979**, *89*, 361−369.
(7) Priyadarshini, D.; Kondratyuk, P.; Picard, Y. N.; Morreale, B. D.; Gellman, A. J.; Miller, J. B. High-Throughput Characterization of Surface Segregation in Cu_xPd_{1-x} Alloys. *J. Phys. Chem. C* **2011**, *115*, 10155−10163.
(8) Cushman, C. V.; Brüner, P.; Zakel, J.; Major, G.; Lunt, B. M.; Grehl, T.; Smith, N. J.; Linford, M. R. A Pictorial View of LEIS and ToF-SIMS Instrumentation. *Vac. Technol. Coating* **2016**, 27−35.
(9) Brongersmal, H. H.; Mu, P. M. Analysis of the Outermost Atomic Layer of a Surface by Low-Energy Ion Scattering. *Surf. Sci.* **1973**, *35*, 393−412.
(10) Tarditi, A. M.; Imhoff, C.; Miller, J. B.; Cornaglia, L. Surface Composition of PdCuAu Ternary Alloys: A Combined LEIS and XPS Study. *Surf. Interface Anal.* **2015**, *47*, 745−754.
(11) Hoffmann, M. A.; Wynblatt, P. Surface Composition of Ternary Cu-Ag-Au Alloys: Part l. Experimental Results. *Metall. Trans. A* **1991**, *22*, 1833−1840.
(12) Jia, H.; Wu, P.; Zeng, G.; Salas-Colera, E.; Serrano, A.; Castro, G. R.; Xu, H.; Sun, C.; Goldbach, A. High-Temperature Stability of Pd Alloy Membranes Containing Cu and Au. *J. Membr. Sci.* **2017**, *544*, 151−160.
(13) Li, J.; Yin, H.-M.; Li, X.-B.; Okunishi, E.; Shen, Y.-L.; He, J.; Tang, Z.-K.; Wang, W.-X.; Yücelen, E.; Li, C.; et al. Surface Evolution of a Pt−Pd−Au Electrocatalyst for Stable Oxygen Reduction. *Nat. Energy* **2017**, *2*, 17111.
(14) Melendez, J.; de Nooijer, N.; Coenen, K.; Fernandez, E.; Viviente, J. L.; van Sint Annaland, M.; Arias, P. L.; Tanaka, D. A. P.; Gallucci, F. Effect of Au Addition on Hydrogen Permeation and the Resistance to H_2S on Pd-Ag Alloy Membranes. *J. Membr. Sci.* **2017**, *542*, 329−341.
(15) Tarditi, A. M.; Cornaglia, L. M. Novel PdAgCu Ternary Alloy as Promising Materials for Hydrogen Separation Membranes: Synthesis and Characterization. *Surf. Sci.* **2011**, *605*, 62−71.
(16) Maclean, D. *Grain Boundaries in Metals*; Clarendon Press: Oxford, U.K., 1957.
(17) Langmuir, I. The Adsorption of Gases on Plane Surfaces of Glass, Mica and Platinum. *J. Am. Chem. Soc.* **1918**, *40*, 1361−1403.
(18) Sachtler, W. M. H.; van Santen, R. A. Surface Composition of Binary Alloys. *Appl. Surf. Sci.* **1979**, *3*, 121−144.
(19) Guttmann, M.; Dumoulin, P.; Wayman, M. The Thermodynamics of Interactive Co-Segregation of Phosphorus and Alloying Elements in Iron and Temper-Brittle Steels. *Metall. Trans. A* **1982**, *13*, 1693−1711.
(20) Hondros, E. D.; Seah, M. P. Theory of Grain Boundary Segregation in Terms of Surface Adsorption Analogues. *Metall. Trans. A* **1977**, *8*, 1363−1371.
(21) Seah, M. Quantitative Prediction of Surface Segregation. *J. Catal.* **1979**, *57*, 450−457.
(22) Boes, J. R.; Kitchin, J. R. Modeling Segregation on AuPd(111) Surfaces with Density Functional Theory and Monte Carlo Simulations. *J. Phys. Chem. C* **2017**, *121*, 3479−3487.
(23) Wynblatt, P.; Landa, A. Computer Simulation of Surface Segregation in Ternary Alloys. *Comput. Mater. Sci.* **1999**, *15*, 250−263.
(24) Good, B.; Bozzolo, G. H.; Abel, P. B. Surface Segregation in Ternary Alloys. *Surf. Sci.* **2000**, *454−456*, 602−607.
(25) Cheng, F.; He, X.; Chen, Z.-X.; Huang, Y.-G. Kinetic Monte Carlo Simulation of Surface Segregation in Pd-Cu Alloys. *J. Alloys Compd.* **2015**, *648*, 1090−1096.
(26) Soto-Verdugo, V.; Metiu, H. Segregation at the Surface of an Au/Pd Alloy Exposed to CO. *Surf. Sci.* **2007**, *601*, 5332−5339.
(27) Boes, J. R.; Gumuslu, G.; Miller, J. B.; Gellman, A. J.; Kitchin, J. R. Estimating Bulk-Composition-Dependent H_2 Adsorption Energies on Cu_xPd_{1-x}(111) Alloy Surfaces. *ACS Catal.* **2015**, *5*, 1020−1026.
(28) Miller, J. B.; Morreale, B. D.; Gellman, A. J. The Effect of Adsorbed Sulfur on Surface Segregation in a Polycrystalline $Pd_{70}Cu_{30}$ Alloy. *Surf. Sci.* **2008**, *602*, 1819−1825.
(29) Yan, X. L.; Wang, J. Y.; Swart, H. C.; Terblans, J. J. AES Study of Cu and S Surface Segregation in a Ternary Ni-Cu(S) Alloy in Combination with a Linear Heating Method. *J. Alloys Compd.* **2018**, *768*, 875−882.
(30) Jeng, S.-P.; Holloway, P. H.; Asbury, D. A.; Hoflund, G. B. Changes Induced at Ni/Cr Alloy Surfaces by Annealing and Oxygen Exposure. *Surf. Sci.* **1990**, *235*, 175−185.
(31) McCue, A. J.; Anderson, J. A. CO Induced Surface Segregation as a Means of Improving Surface Composition and Enhancing Performance of CuPd Bimetallic Catalysts. *J. Catal.* **2015**, *329*, 538−546.
(32) Plessis, J. d.; van Wyk, G. N. A model for surface segregation in multicomponent alloys—part V: The kinetics of surface segregation in multicomponent alloys. *J. Phys. Chem. Solid.* **1989**, *50*, 251−257.
(33) Takeuchi, I.; Famodu, O. O.; Read, J. C.; Aronova, M. A.; Chang, K.-S.; Craciunescu, C.; Lofland, S. E.; Wuttig, M.; Wellstood, F. C.; Knauss, L.; et al. Identification of Novel Compositions of Ferromagnetic Shape-Memory Alloys Using Composition Spreads. *Nat. Mater.* **2003**, *2*, 180−184.
(34) Long, C. J.; Hattrick-Simpers, J.; Murakami, M.; Srivastava, R. C.; Takeuchi, I.; Karen, V. L.; Li, X. Rapid Structural Mapping of Ternary Metallic Alloy Systems Using the Combinatorial Approach and Cluster Analysis. *Rev. Sci. Instrum.* **2007**, *78*, 072217.
(35) Hattrick-Simpers, J. R.; Gregoire, J. M.; Kusne, A. G. Perspective: Composition-Structure-Property Mapping in High-Throughput Experiments: Turning Data into Knowledge. *APL Mater* **2016**, *4*, 053211.
(36) Green, M. L.; Takeuchi, I.; Hattrick-Simpers, J. R. Applications of High Throughput (Combinatorial) Methodologies to Electronic, Magnetic, Optical, and Energy-Related Materials. *J. Appl. Phys.* **2013**, *113*, 231101.
(37) Kitchin, J. R.; Gellman, A. J. High-Throughput Methods Using Composition and Structure Spread Libraries. *AIChE J.* **2016**, *62*, 3826.
(38) Gainullin, I. K. Towards Quantitative LEIS with Alkali Metal Ions. *Surf. Sci.* **2018**, *677*, 324−332.
(39) Yin, C.; Miller, J. B.; Kondratyuk, P.; Gellman, A. J. Detection of CuAuPd Phase Boundaries Using Core Level Shifts. *J. Phys. Chem. B* **2018**, *122*, 764−769.
(40) Fleutot, B.; Miller, J. B.; Gellman, A. J. Apparatus for Deposition of Composition Spread Alloy Films: The Rotatable Shadow Mask. *J. Vac. Sci. Technol., A* **2012**, *30*, 061511.
(41) Sárkány, A.; Geszti, O.; Sáfrán, G. Preparation of Pd shell-Au core/SiO_2 catalyst and Catalytic Activity for Acetylene Hydrogenation. *Appl. Catal., A* **2008**, *350*, 157−163.
(42) McCue, A. J.; Shepherd, A. M.; Anderson, J. A. Optimisation of Preparation Method for Pd Doped Cu/Al_2O_3 Catalysts for Selective Acetylene Hydrogenation. *Catal. Sci. Technol.* **2015**, *5*, 2880−2890.
(43) Wang, H.; Yin, S.; Li, Y.; Yu, H.; Li, C.; Deng, K.; Xu, Y.; Li, X.; Xue, H.; Wang, L. One-Step Fabrication of Tri-Metallic PdCuAu

https://dx.doi.org/10.1021/acs.jpcc.0c02058
J. Phys. Chem. C 2020, 124, 10605−10614

Nanothorn Assemblies as an Efficient Catalyst for Oxygen Reduction Reaction. *J. Mater. Chem. A* **2018**, *6*, 3642−3648.
(44) Zhang, K.; Way, J. D. Palladium-Copper Membranes for Hydrogen Separation. *Sep. Purif. Technol.* **2017**, *186*, 39−44.
(45) Hatlevik, Ø.; Gade, S. K.; Keeling, M. K.; Thoen, P. M.; Davidson, A. P.; Way, J. D. Palladium and Palladium Alloy Membranes for Hydrogen Separation and Production: History, Fabrication Strategies, and Current Performance. *Sep. Purif. Technol.* **2010**, *73*, 59−64.
(46) Adhikari, S.; Fernando, S. Hydrogen Membrane Separation Techniques. *Ind. Eng. Chem. Res.* **2006**, *45*, 875−881.
(47) Scott, F. M. The Construction of Palladium and Palladium-Alloy Supported Membranes for Hydrogen Separation Using Supercritical Fluid Deposition. Ph.D. Thesis, University of Massachusetts Amherst, 2004.
(48) Edlund, D. J.; McCarthy, J. The Relationship between Intermetallic Diffusion and Flux Decline in Composite-Metal Membranes: Implications for Achieving Long Membrane Lifetime. *J. Membr. Sci.* **1995**, *107*, 147−153.
(49) Ishihara, T.; Kawahara, A.; Fukunaga, A.; Nishiguchi, H.; Shinkai, H.; Miyaki, M.; Takita, Y. CH_4 Decomposition with a Pd−Ag Hydrogen-Permeating Membrane Reactor for Hydrogen Production at Decreased Temperature. *Ind. Eng. Chem. Res.* **2002**, *41*, 3365−3369.
(50) Roa, F.; Block, M. J.; Way, J. D. The Influence of Alloy Composition on the H_2 Flux of Composite Pd-Cu Membranes. *Desalination* **2002**, *147*, 411.
(51) Basile, A. Hydrogen Production Using Pd-Based Membrane Reactors for Fuel Cells. *Top. Catal.* **2008**, *51*, 107−122.
(52) Amandusson, H.; Ekedahl, L.; Dannetun, H. Hydrogen Permeation Through Surface Modified Pd and PdAg Membranes. *J. Membr. Sci.* **2001**, *193*, 35−47.
(53) Guerreiro, H.; Manuel, B. Palladium−Copper−Gold Alloys for the Separation of Hydrogen Gas. Ph.D. Thesis, Université du Québec, 2015, p 216.
(54) Honrado Guerreiro, B.; Martin, M. H.; Roué, L.; Guay, D. Hydrogen Solubility of Magnetron Co-Sputtered FCC and BCC PdCuAu Thin Films. *J. Phys. Chem. C* **2016**, *120*, 5297−5307.
(55) Sharpe, R.; Counsell, J.; Bowker, M. Pd Segregation to the Surface of Au on Pd(111) and on Pd/TiO_2(110). *Surf. Sci.* **2017**, *656*, 60−65.
(56) Dalla Fontana, A.; Sirini, N.; Cornaglia, L. M.; Tarditi, A. M. Hydrogen Permeation and Surface Properties of PdAu and PdAgAu Membranes in the Presence of CO, CO_2 and H_2S. *J. Membr. Sci.* **2018**, *563*, 351−359.
(57) Gao, F.; Goodman, D. W. Pd-Au Bimetallic Catalysts: Understanding Alloy Effects from Planar Models and (Supported) Nanoparticles. *Chem. Soc. Rev.* **2012**, *41*, 8009−8020.
(58) Chen, M.; Goodman, D. W. Promotional Effects of Au in Pd-Au Catalysts for Vinyl Acetate Synthesis. *Chin. J. Catal.* **2008**, *29*, 1178−1186.
(59) Yi, C.-W.; Luo, K.; Wei, T.; Goodman, D. W. The Composition and Structure of Pd-Au Surfaces. *J. Phys. Chem. B* **2005**, *109*, 18535−18540.
(60) Swartzfager, D. G.; Ziemecki, S. B.; Kelley, M. J. Differential Sputtering and Surface Segregation: The Role of Enhanced Diffusion. *J. Vac. Sci. Technol.* **1981**, *19*, 185−191.
(61) Yuan, L.; Goldbach, A.; Xu, H. Segregation and H_2 Transport Rate Control in Body-Centered Cubic PdCu Membranes. *J. Phys. Chem. B* **2007**, *111*, 10952−10958.
(62) Beikler, R.; Taglauer, E. Ion Scattering Studies of Ordered Alloy Surfaces: CuAu(100) and NiAl. *Nucl. Instrum. Methods Phys. Res., Sect. B* **2000**, *161*−*163*, 390−395.
(63) Buck, T. M.; Wheatley, G. H.; Marchut, L. Order-Disorder and Segregation Behavior at the Cu_3Au (001) Surface. *Phys. Rev. Lett.* **1983**, *51*, 43−46.
(64) Bochvar, N.; Liberov, Y. Gold−Copper−Palladium. In *Noble Metal Systems: Selected Systems from Ag−Al−Zn to Rh−Ru−Sc*; Springer Berlin: Heidelberg, 2006; pp 213−225.
(65) Subramanian, P. R.; Laughlin, D. E. Cu-Pd (Copper-Palladium). *J. Phase Equilib.* **1991**, *12*, 231−243.
(66) Boes, J. R.; Kondratyuk, P.; Yin, C.; Miller, J. B.; Gellman, A. J.; Kitchin, J. R. Core Level Shifts in Cu-Pd Alloys as a Function of Bulk Composition and Structure. *Surf. Sci.* **2015**, *640*, 127−132.
(67) Kamakoti, P.; Morreale, B. D.; Ciocco, M. V.; Howard, B. H.; Killmeyer, R. P.; Cugini, A. V.; Sholl, D. S. Prediction of Hydrogen Flux through Sulfur-Tolerant Binary Alloy Membranes. *Science* **2005**, *307*, 569−573.
(68) Braun, F.; Miller, J. B.; Gellman, A. J.; Tarditi, A. M.; Fleutot, B.; Kondratyuk, P.; Cornaglia, L. M. PdAgAu Alloy with High Resistance to Corrosion by H_2S. *Int. J. Hydrogen Energy* **2012**, *37*, 18547−18555.
(69) Beikler, R.; Taglauer, E. Surface Segregation at the Binary Alloy CuAu (100) Studied by Low-Energy Ion Scattering. *Surf. Sci.* **2016**, *643*, 138−141.
(70) Taglauer, E.; Beikler, R. Surface Segregation Studied by Low-Energy Ion Scattering: Experiment and Numerical Simulation. *Vacuum* **2004**, *73*, 9−14.
(71) Smith, D. P. Scattering of Low-Energy Noble Gas Ions from Metal Surfaces. *J. Appl. Phys.* **1967**, *38*, 340−347.
(72) Szanyi, J.; Kuhn, W. K.; Goodman, D. W. CO Adsorption on Pd(111) and Pd(100): Low and High Pressure Correlations. *J. Vac. Sci. Technol., A* **1993**, *11*, 1969−1974.
(73) Seah, M. P.; Hondros, E. D. Grain Boundary Segregation. *Proc. R. Soc. A* **1973**, *335*, 191−212.
(74) Sluiter, M. H. F.; Colinet, C.; Pasturel, A. Ab Initio Calculation of the Phase Stability in Au-Pd and Ag-Pt Alloys. *Phys. Rev. B: Condens. Matter Mater. Phys.* **2006**, *73*, 174204.
(75) Okamoto, H.; Massalski, T. B. The Au-Pd (Gold-Palladium) System. *Bull. Alloy Phase Diagrams* **1985**, *6*, 229−235.
(76) Yu, X.; Gellman, A. J. Suppression of B2 Phase in Pd_zCu_{1-z} Alloy Thin Films. *Thin Solid Films* **2018**, *668*, 50−55.
(77) Priyadarshini, D.; Kondratyuk, P.; Picard, Y. N.; Morreale, B. D.; Gellman, A. J.; Miller, J. B. High-Throughput Characterization of Surface Segregation in Cu_xPd_{1-x} Alloys. *J. Phys. Chem. C* **2011**, *115*, 10155−10163.
(78) Newton, M. A.; Francis, S. M.; Bowker, M. Copper-Palladium Alloy Surfaces. II. Equilibrium Surface Compositions of Dilute Pd/Cu Alloys from a Simple Segregation Model. *Surf. Sci.* **1991**, *259*, 56−64.
(79) Loboda-Cackovic, J.; Mousa, M.; Block, J. Surface Analysis of the PdCu(110) Single Crystal Alloy at Different Segregation Rates. *Vacuum* **1995**, *46*, 89−96.
(80) Miller, J. B.; Matranga, C.; Gellman, A. J. Surface Segregation in a Polycrystalline $Pd_{70}Cu_{30}$ alloy Hydrogen Purification Membrane. *Surf. Sci.* **2008**, *602*, 375−382.
(81) Mårtensson, N.; Nyholm, R.; Calén, H.; Hedman, J.; Johansson, B. Electron-Spectroscopic Studies of the Cu_xPd_{1-x} Alloy System: Chemical-Shift Effects and Valence-Electron Spectra. *Phys. Rev. B: Condens. Matter Mater. Phys.* **1981**, *24*, 1725−1738.
(82) Okamoto, H.; Chakrabarti, D. J.; Laughlin, D. E.; Massalski, T. B. The Au-Cu (Gold-Copper) System. *J. Phase Equilib.* **1987**, *8*, 454.
(83) Vasiliev, M. A. Surface Effects of Ordering in Binary Alloys. *J. Phys. D: Appl. Phys.* **1997**, *30*, 3037−3070.
(84) McRae, E. G.; Buck, T. M.; Malic, R. A.; Wallace, W. E.; Sanchez, J. M. Ordering and Layer Composition at the Cu_3Au(110) Surface. *Surf. Sci.* **1990**, *238*, L481.
(85) Potter, H. C.; Blakely, J. M. LEED, Auger Spectroscopy, and Contact Potential Studies of Copper-Gold Alloy Single Crystal Surfaces. *J. Vac. Sci. Technol.* **1975**, *12*, 635−642.

https://dx.doi.org/10.1021/acs.jpcc.0c02058
J. Phys. Chem. C 2020, 124, 10605−10614